Numerical Solutions for the Flowfield Around a Counter-Rotating Propeller

Makoto Kobayakawa* and Masahiro Nakao†
Kyoto University, Kyoto, Japan

Three-dimensional Euler equations are used to investigate the flowfield around a counter-rotating propeller in flight at a Mach 0.8. Two volumes including front and rear blades are solved separately. The interaction between both blades is included in the calculation by the connecting surfaces. The non-iterative implicit ADI (alternating direction implicit) scheme is used in order to solve the Euler equations. The periodic steady solution is obtained. This simulates the relative motion of the blades exactly. Numerical calculations are performed for a counter-rotating propfan with SR-3 blade configurations. The results show that the propeller efficiency is superior to that of a single-rotating propfan with the same number of blades.

Nomenclature

A,B,C	= Jacobian matrices
b	= blade chord
C_p	= pressure coefficient, $(p-p_\infty)/(1/2\rho_\infty V_\infty^2)$
c	= local speed of sound, $(\gamma p/\rho)^{1/2}$
e	= total energy per unit volume
e_e,e_i	= explicit and implicit smoothing coefficients
E,F,G	= vectors of flux quantities in z-, r- and ϕ-directions
H	= vector of source term created by cylindrical coordinate transformation
J	= Jacobian of coordinate transformation or advance ratio
$k_i,k=0,3$	= generalized matrices defined in Eq. (7)
p	= static pressure
Q	= dependent variable vector
R	= blade radius
U,V,W	= contravariant velocity components defined in Eq. (3)
u,v,w	= velocities in z-, r- and ϕ-directions
V_∞	= freestream velocity
z,r,ϕ	= physical space coordinates
γ	= ratio of specific heats
ρ	= air density
ξ,η,ζ	= computational space coordinates
Ω	= angular velocity of rotation

Subscripts

i,j,k	= mesh point location along ξ-, η- and ζ-directions
∞	= freestream condition
$\hat{}$	= value in computational space

I. Introduction

STUDIES and developments of propfan powered aircraft are in progress throughout the world. Indeed, flight test for practical use is already realized in the U.S.

Of the several advantages of a theoretical investigation of propfan aerodynamic performance, the most prominent one is the ability to obtain the flow detail around very complex configurations. Such detail is difficult to obtain from wind tunnel tests. Potential and Euler equations are available for the numerical aerodynamic calculations and some results have already been obtained for single-rotating propfans.[1-4] However, many propfans may be counter-rotating pusher types, and, therefore, their flowfield and performance will differ considerably from those of single rotating tractor type. No published results have been found concerning numerical aerodynamic calculations for the counter-rotating propfan.

In this paper, the Euler equations for the flowfield around a counter-rotating propeller are solved by extending the numerical techniques applied to a singe-rotating propfan.[4] The implicit finite difference scheme is used in order to solve the Euler equations.

II. Basic Equations

Let the system of cylindrical coordinates be defined as shown in Fig. 1. The unsteady Euler equation in weak conservation law form is transformed into the following equation in the computational domain.

$$\hat{Q}_\tau + \hat{E}_\xi + \hat{F}_\eta + \hat{G}_\zeta + \hat{H} = 0 \tag{1}$$

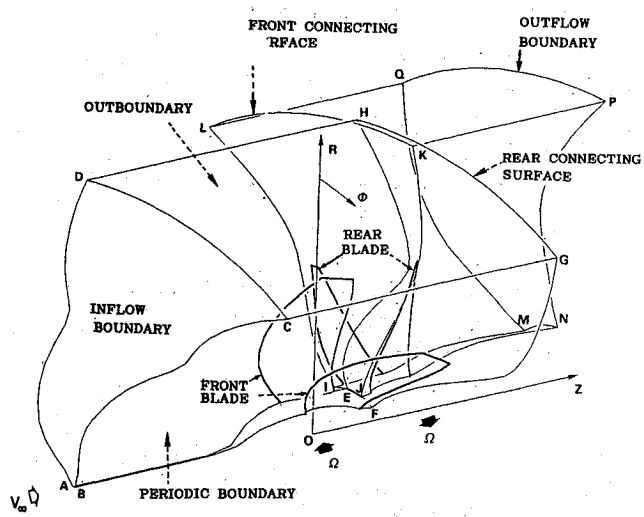

Fig. 1 Physical space and cylindrical coordinates.

Received April 27, 1987; revision received Oct. 30, 1987.

*Associate Professor. Member AIAA.
†Graduate Student; currently, Research Engineer, Mitsubishi Heavy Industry Co. Ltd., Nagoya, Japan.

where

$$\hat{Q} = J^{-1}\begin{bmatrix}\rho\\ \rho u\\ \rho v\\ \rho w\\ e\end{bmatrix} \qquad \hat{E} = J^{-1}\begin{bmatrix}\rho U\\ \rho uU + p\xi_z\\ \rho vU + p\xi_r\\ \rho wU + p\xi_\phi/r\\ (e+p)U - p\xi_t\end{bmatrix}$$

$$\hat{F} = J^{-1}\begin{bmatrix}\rho V\\ \rho uV + p\eta_z\\ \rho vV + p\eta_r\\ \rho wV + p\eta_\phi/r\\ (e+p)V - p\eta_t\end{bmatrix} \qquad \hat{G} = J^{-1}\begin{bmatrix}\rho W\\ \rho uW + p\zeta_z\\ \rho vW + p\zeta_r\\ \rho wW + p\zeta_\phi/r\\ (e+p)W - p\zeta_t\end{bmatrix}$$

$$\hat{H} = J^{-1}/r\begin{bmatrix}\rho v\\ \rho uv\\ \rho(v^2 - w^2)\\ 2\rho vw\\ (e+p)v\end{bmatrix} \tag{2}$$

$$U = \xi_t + u\xi_z + v\xi_r + w\xi_\phi/r$$

$$V = \eta_t + u\eta_z + v\eta_r + w\eta_\phi/r$$

$$W = \zeta_t + u\zeta_z + v\zeta_r + w\zeta_\phi/r \tag{3}$$

The transformation of cylindrical coordinates in physical space into generalized nonorthogonal coordinates is performed by

$$\tau = t$$

$$\xi = \xi(t,z,r,\phi)$$

$$\eta = \eta(t,z,r,\phi)$$

$$\zeta = \zeta(t,z,r,\phi) \tag{4}$$

This transformation maps the nacelle surface into a constant η-plane and both sides of the blades into two constant ζ-planes, as shown in Fig. 2. The detailed form of J and derivatives ξ_t, ξ_z, etc. are given in Refs. 1 and 2.

Furthermore, u, v and w and the pressure and density are nondimensionalized by $a_\infty\sqrt{\gamma}$, p_∞ and ρ_∞, respectively, and, z and r are nondimensionalized by R.

III. Mesh Generation

As shown in Fig. 1, the counter-rotating propfan has two sets of blades with opposite directions of rotation. Since the Euler equation (1) is written for a space fixed frame, the mesh systems in the physical space rotate in the numerical calculations. Therefore, a unified mesh system cannot be generated for a pair of front and rear blades. Thus, two mesh systems, divided by two connecting surfaces, are generated.

Both meshes are expanded on the space between neighboring blades and the space including the front blade is surrounded by an inflow boundary, out boundary, and outflow boundary (rear connecting surface). The space including the rear blade is surrounded by an inflow boundary (front connecting surface), out boundary and outflow boundary. The connecting surfaces are located between the two blades.

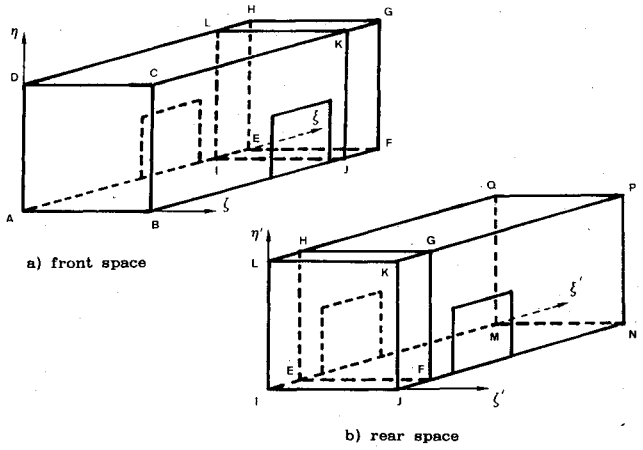

Fig. 2 Computational spaces.

The method described in Ref. 4 is utilized as the grid generation procedure. Basically, an H-type mesh is used around the sectional form of the blade. However, since the pitch angles differ considerably from the front blade to the rear blade, the mesh lines are connected smoothly during this domain. As described before, the two meshes rotate in opposite directions and the connecting surfaces must be axisymmetric around the axis of rotation. Figure 3 shows examples of generated mesh lines of a counter-rotating propfan using SR-3 as blade configuration.

IV. Method of Numerical Calculations

The numerical algorithm used to solve the transformed Euler equation (which has the weak conservation law form) is a non-iterative, implicit ADI scheme.[5] However, for the counter-rotating propfan, the space including the front blade (front space) rotates in the opposite direction of the space including the rear blade (rear space) bounded by the connecting surfaces (see Fig. 3b). Since the finite difference equations cannot be inverted at one time, the following two steps are taken in this calculation.[6]

A. Front Flowfield

In the front space, the flowfield between the inflow boundary and the rear connecting surface is calculated. Except for those on the boundaries, the values can be obtained by solving Eq. (1). An implicit approximate-factorization scheme for Eq. (1) takes the following well known form.

$$\begin{aligned}&[I + \Delta t\delta_\xi\hat{A}^n - e_i(J^{-1}\nabla_\xi\Delta_\xi J)^n]\\ &\times [I + \Delta t\delta_\eta\hat{B}^n - e_i(J^{-1}\nabla_\eta\Delta_\eta J)^n]\\ &\times [I + \Delta t\delta_\zeta\hat{C}^n - e_i(J^{-1}\nabla_\zeta\Delta_\zeta J)^n](Q^{n+1} - Q^n)\\ &= -\Delta t(\delta_\xi\hat{E}^n + \delta_\eta\hat{F}^n + \delta_\zeta\hat{G}^n + \hat{H}^n) - e_e J^{-1}[(\nabla_\xi\Delta_\xi)^2\\ &+ (\nabla_\eta\Delta_\eta)^2 + (\nabla_\zeta\Delta_\zeta)^2](J\hat{Q})^n\end{aligned} \tag{5}$$

where $\hat{A}$, $\hat{B}$ and $\hat{C}$ are Jacobian matrices in the computational space related to those in physical space as follows:

$$\hat{A} = \partial\hat{E}/\partial\hat{Q} = k_0 I + k_1 A + k_2 B + \frac{k_3}{r}C \tag{6}$$

for

$$k_0 = \xi_t,\ k_1 = \xi_z,\ k_2 = \xi_r,\ k_3 = \xi_\phi \tag{7}$$

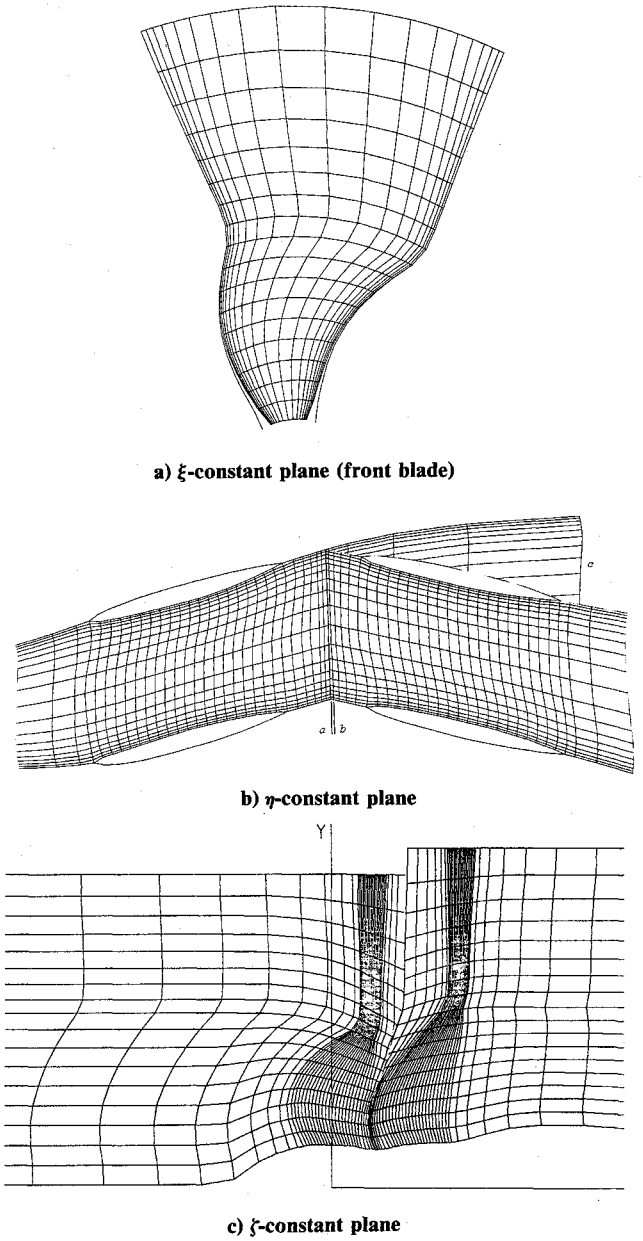

a) ξ-constant plane (front blade)

b) η-constant plane

c) ζ-constant plane

Fig. 3 Mesh generated around a counter-rotating propfan with SR-3 blade configuration.

In order to get a stable solution in a transonic flowfield, the difference scheme should be switched, depending upon whether the flow velocity is subsonic or supersonic. In this case, only δ_ξ is calculated using Eqs. (28) and (29) in Ref. 5. By this procedure the differencing scheme transfers from a central difference one to an upwind one smoothly as the flow velocity changes from subsonic to supersonic. The other differentiations δ_η and δ_ζ are approximated by the central difference.

In order to solve Eq. (5), the following four sequential processes are performed.

$$[I + \Delta t \delta_\xi \hat{A}^n - e_i(J^{-1}\nabla_\xi \Delta_\xi J)^n]\Delta\hat{Q}^* = RHS^n$$

$$[I + \Delta t \delta_\eta \hat{B}^n - e_i(J^{-1}\nabla_\eta \Delta_\eta J)^n]\Delta\hat{Q}^{**} = \Delta\hat{Q}^*$$

$$[I + \Delta t \delta_\zeta \hat{C}^n - e_i(J^{-1}\nabla_\zeta \Delta_\zeta J)^n]\Delta\hat{Q}^n = \Delta\hat{Q}^{**}$$

$$\hat{Q}^{n+1} = \hat{Q}^n + \Delta\hat{Q}^n \tag{8}$$

where $\Delta\hat{Q}^*$ and $\Delta\hat{Q}^{**}$ are intermediate values of the first and second inversions, respectively. For finite difference calculations, first order accuracy is applied for Δt and second order accuracy for the space differencing.

Boundary conditions of the first step are given as follows:

1. Inflow and Out Boundaries

$$\Delta\hat{Q}_{ABCD} = \Delta\hat{Q}_{CGHD} = 0 \tag{9}$$

2. Rear Connecting Surface

The outflow conditions of the first step is given on the rear connecting surface. The grid points of the connecting surface in the windward side slip from those in the leeward side as the front and rear blades rotate in the opposite direction. The values of the grid points in the windward side are interpolated from the grid points in the leeward side (Fig. 3b).

3. Tangency Conditions on the Solid Surfaces

$$W = 0\text{: blade}$$

$$V = 0\text{: nacelle}$$

$$V = W = 0\text{: intersection of blade and nacelle} \tag{10}$$

Nonzero contravariant velocity components are obtained by linear extrapolation on the solid surface. The velocities in physical space u, v and w are, therefore, calculated by the following equations.

$$\begin{bmatrix} u \\ v \\ w \end{bmatrix} =$$

$$J^{-1}\begin{bmatrix} (\eta_r\zeta_\phi - \eta_\phi\zeta_r)/r & -(\xi_r\zeta_\phi - \xi_\phi\zeta_r)/r & (\xi_r\eta_\phi - \xi_\phi\eta_r)/r \\ -(\eta_z\zeta_\phi - \eta_\phi\zeta_z)/r & (\xi_z\zeta_\phi - \xi_\phi\zeta_r)/r & -(\xi_z\eta_\phi - \xi_\phi\eta_r)/r \\ (\eta_z\zeta_r - \eta_r\zeta_z) & -(\xi_z\zeta_r - \xi_r\zeta_z) & (\xi_z\eta_r - \xi_r\eta_z) \end{bmatrix}$$

$$\begin{bmatrix} U - \xi_t \\ V - \eta_t \\ W - \zeta_t \end{bmatrix} \tag{11}$$

4. Periodic Boundaries

The periodic boundaries are located at the outside parts of the suction and pressure sides of the blade. The values of two points that correspond with each other should be equal to those on the periodic boundaries.

$$\Delta\hat{Q}_{AEHD} = \Delta\hat{Q}_{BFGC} \tag{12}$$

B. Rear Flowfield

In the rear space, the flowfield between the front connecting surface (Fig. 3b) and the outflow boundary is calculated. The algorithm is the same as the first step and abbreviated in this section. The values at the front connecting surface are obtained by interpolation from the front grid points. Furthermore, the values on the outflow boundary are obtained by assuming $\Delta p = 0$ and by linear extrapolation if the flow is supersonic.

C. Calculation Procedures

The calculations are performed in the following steps[6]:

1) $t = 0$: Uniform flow is set.

2) $t = \Delta t$: First, the front flowfield is solved. At the out-

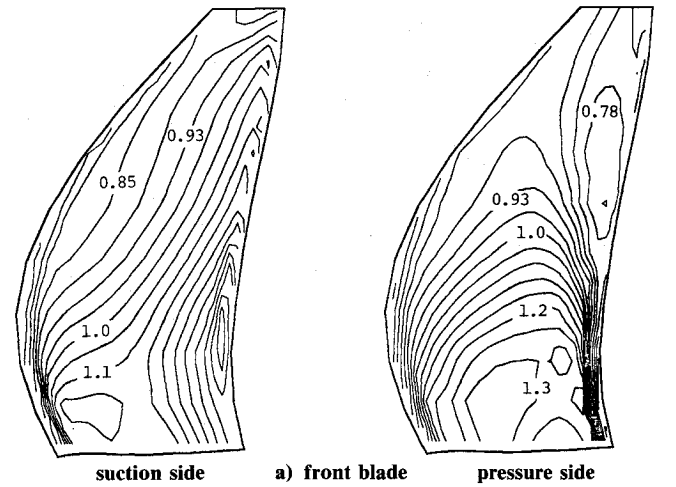

Fig. 4 Iso-Mach lines on the blades.

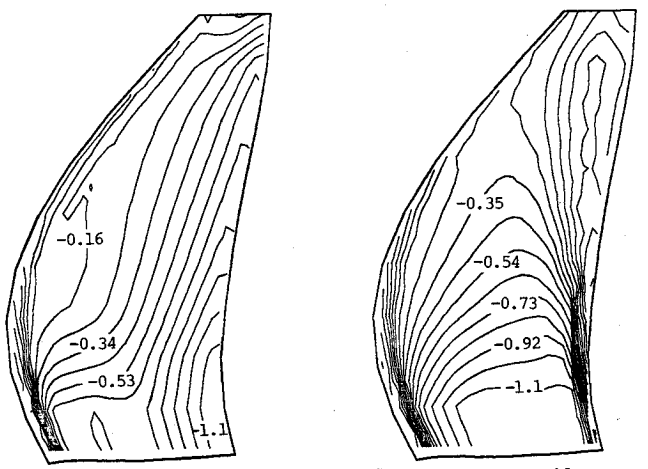

Fig. 5 Isobar lines on the blades.

flow boundary in the fictitious mesh system (see Fig. 3b), the uniform flow condition is given, Next, the rear flowfield is solved. At the inflow boundary (front connecting surface), the values of the static variables obtained in the first step are given.

3) $t = 2\Delta t$: First, the front flowfield is solved. At the outflow boundary (rear connecting surface), the values of variables obtained in the step 2 ($t = \Delta t$) are given. Next, the rear flowfield is solved. At the inflow boundary (front connecting surface), the values of variables obtained in the first step of this time level are given.

$(N + 1)\ t = N\Delta t$: First, the front flowfield is solved. At the outflow boundary (rear connecting surface), the values of variables obtained in the step N $[t = (N - 1)\Delta t]$ are given. Next, the rear flowfield is solved. At the inflow boundary (front connecting surface), the values of variables obtained in the first step of this time level are given.

The time duration of $(N + 1)\Delta t$ means one period of the relative motion of two blades, i.e., the same relative situation between the front and rear blades, occurs after $(N + 1)\Delta t$. The data from one period are compared to data in a previous one, and if ΔQ at each stage becomes smaller than the specified correction value, the calculation is considered to be converged.

V. Numerical Results and Discussions

The numerical calculations are performed for the counter-rotating propfan described in Sec. III. The pitch angle at three quarters of the tip radius is 57.3 deg, the advance ratio is 3.4 and the flight Mach number is 0.8. The number of meshes are 38 along the z-direction, 18 along the r-direction and 19 along the ϕ-direction for the front space, and 39, 18 and 19 for the rear space, respectively. The distance between the front and rear blades is $0.475R$. When dissipation coefficients e_i and e_e were 1.0 and 0.04, respectively, the calculation converged at a time step of 0.01. Therefore, one period is divided into 40 time steps.

Lines of constant relative Mach number and pressure on the suction and pressure sides of the blades are shown in Figs. 4 and 5, respectively. These quantities are shown also for the regions above and below the blades in Figs. 6 and 7. These figures show that shock waves appear on the suction side of the rear blade and on the pressure side of the front blade, and the patterns of iso-Mach and isobar lines are different between the front and rear blades. Especially on the rear part of the suction side of the front blade, supersonic flow is observed and it continues until the trailing edge, and on the pressure side, a supersonic region appears. It is hypothesized that this is because the induced flow from the rear blade causes the angle of attack of the front blade to become negative. Furthermore, the nacelle configuration of this example affects the flowfield on the blades. The iso-Mach and isobar lines on the rear blade resemble those of the single rotation blade.

The velocity vectors on the connecting surface and the surface behind the trailing edge of the rear blade are depicted in Figs. 8 and 9, respectively. In these figures, the tip vortices are clearly seen.

Efficiency and power coefficient are 0.833 and 0.94, respectively, while those of the single rotation system are 0.776 and 0.99. This fact shows that aerodynamic performance is improved by the counter-rotation system. Comparing this to the experimental results in Fig. 23 of Ref. 7, the experiments

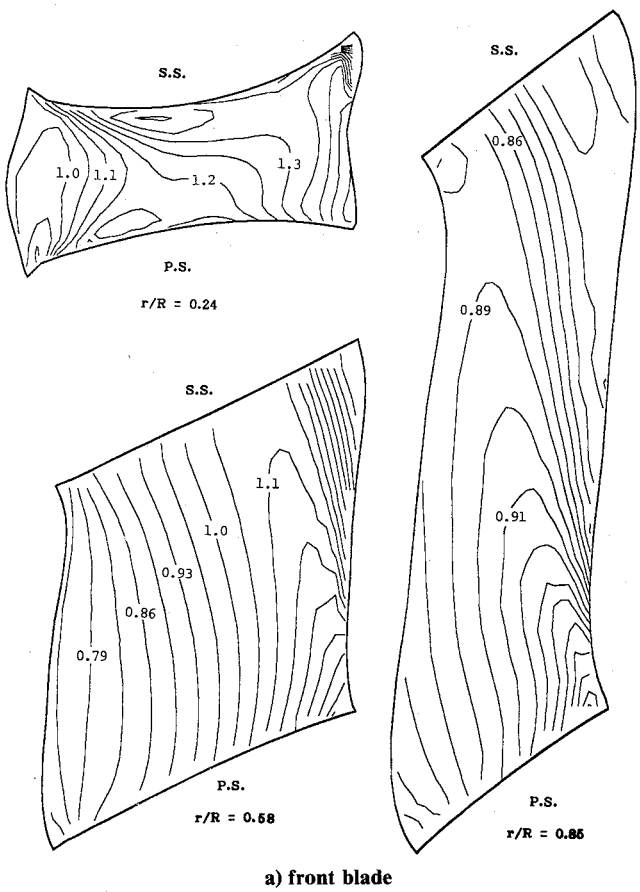

a) front blade

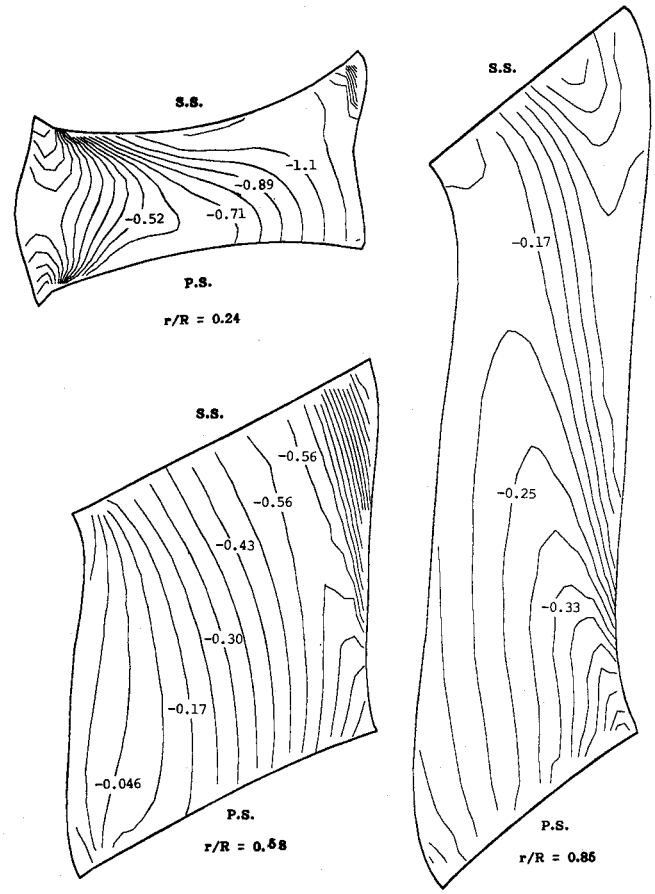

a) front blade

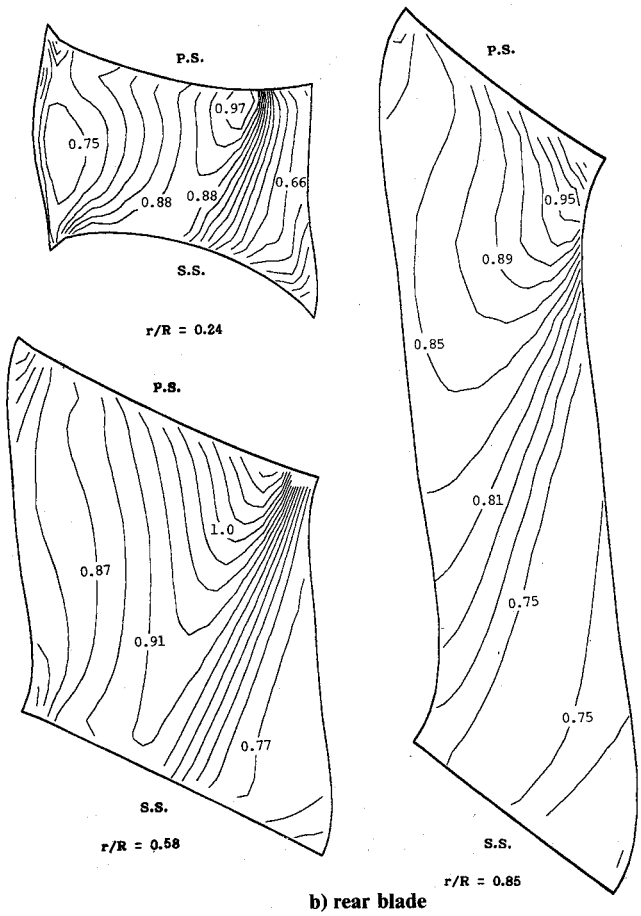

b) rear blade

Fig. 6 Iso-Mach lines between the blades.

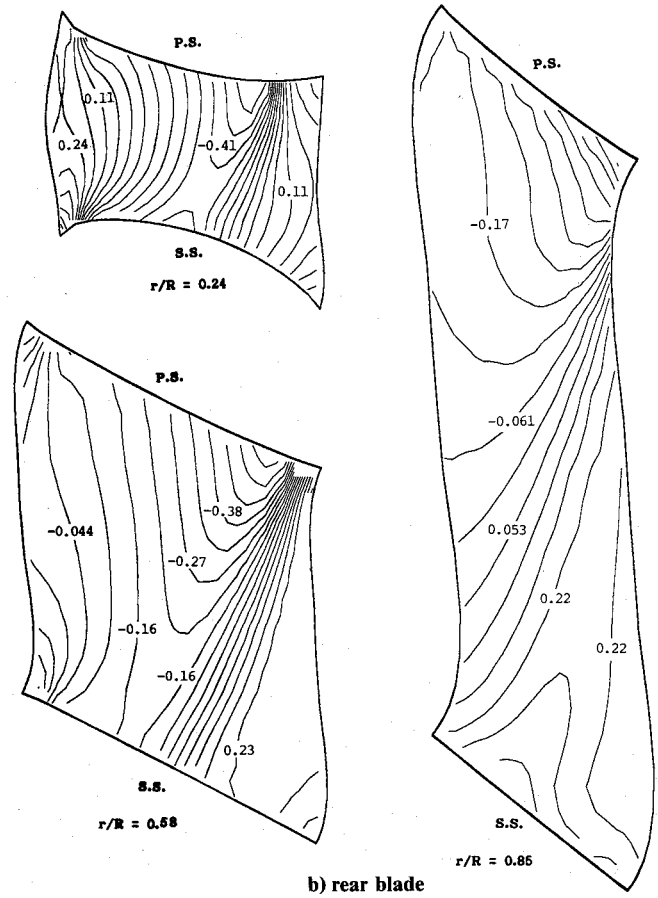

b) rear blade

Fig. 7 Isobar lines between the blades.

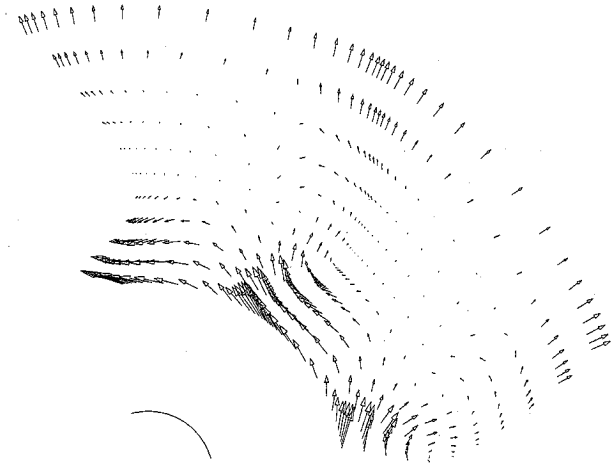

Fig. 8 Velocity vectors on the connecting surface.

Fig. 9 Velocity vectors behind the rear blade.

indicate the 6% superiority of the net efficiency of counter-rotation from single one, which is close to this analysis. However, the number of grid points used are too few for the quantitative estimation of the performance of a counter-rotating propfan, these results should be regarded as qualitatively useful.

VI. Concluding Remarks

It is very important to investigate the flowfield around a propfan for its optimal design. In order to accomplish this, numerical methods are necessary, as appropriate wind tunnel tests might be difficult. Among several numerical techniques, the three-dimensional Euler equations are most promising for this purpose. The flowfield around a counter-rotating propfan in flight at a Mach number of 0.8 is solved. In this analysis, cylindrical coordinates are employed. The flowfield in two spaces including front and rear blades rotating in the opposite directions are solved separately. The interaction between both blade sets are taken into account in the calculation by the connecting surfaces.

The noniterative implicit ADI scheme is used in order to solve the Euler equations. The periodic steady state solutions are obtained by rotating the space including the front blade and the space including the rear blade in the opposite directions. The results show that the distribution of Mach number around the front blade becomes high due to the induced flow from the rear blade. All variables vary in a sinusoidal manner that is regarded as the periodic steady state. The calculated efficiency of the counter-rotating propfan is superior for about 6% than that of single-rotating propfan. This agrees well with the experimental result. However, since the number of the grid points are too few for the quantitative estimation, this result should be regarded as only qualitatively useful.

Acknowledgments

The authors express their thanks to Professors H. Foersching and W. Geissler of DFVLR for helpful discussions throughout this research.

References

[1]Chaussee, D. S. and Kutler, P., "User's Manual for Three-Dimensional Analysis of Propeller Flow Fields," NASA CR-167959, Jan. 1983.

[2]Bober, L. J., Chaussee, D. S., Kutler, P., "Prediction of High Speed Propeller Flow Fields Using a Three-Dimensional Euler Analysis," AIAA Paper 83-0188, Jan. 1983.

[3]Bousquet, J. M., "Methodes Aerodynamiques Utilisees en France pour L'etude des Helices pour Avions Rapides," *La Recherche Aerospaciale,* Jan.-Feb. 1985, pp. 1-15.

[4]Kobayakawa, M., Onuma, H., and Shiota, Y., "Calculations of High Speed Propeller Performances Using Finite Difference Methods," *Proceedings of the 15th International Council of the Aeronautical Sciences,* AIAA, New York, 1986, pp. 1451-1458.

[5]Beam, R. M. and Warming, R. F., "An Implicit Finite-Difference Algorithm for Hyperbolic Systems in Conservation-Law Form," *Journal of Computational Physics,* Vol. 22, Sept. 1976, pp. 87-110.

[6]Koya, M. and Kotake, S., "Numerical Analysis of Fully Three-Dimensional Periodic Flows Through a Turbine Stage," *Journal of Engineering for Gas Turbines and Power,* Vol. 107, Oct. 1985, pp. 945-952.

[7]Wainauski, H. S. and Vaczy, C. M., "Aerodynamic Performance of a Counter Rotating Prop-Fan," AIAA Paper 86-1550, June 1986.